Science Advances
AAAS

Supplementary Materials for

Bioaerosols are the dominant source of warm-temperature immersion-mode INPs and drive uncertainties in INP predictability

Gavin C. Cornwell *et al.*

Corresponding author: Gavin C. Cornwell, gavin.cornwell@pnnl.gov

Sci. Adv. **9**, eadg3715 (2023)
DOI: 10.1126/sciadv.adg3715

This PDF file includes:

Supplementary Text

Aerosol modeling in E3SM

Sea spray and dust aerosol source functions were simulated using the Energy Exascale Earth System Model version 1 (E3SMv1; (*79*)). The E3SM Atmosphere Model version 1 (EAMv1; (*80*)) is the atmospheric component of E3SM. EAMv1 has a horizontal grid spacing of ca.~110~km in standard resolution, with 72~vertical levels between the surface and the tropopause. The land surface model was configured to use prescribed seasonally-varying vegetation fields (*81*).

EAMv1 simulations were run at standard resolution using meteorological input fields from 2014-06-01 to 2015-12-01. Specifically, in order to match the meteorology of the observed time period, we nudge the simulated winds towards the Modern Era Retrospective-Analysis for Research and Applications reanalysis product (MERRA-2) (*82*). Our nudging implementation follows (*83*), and the impacts of different nudging strategies in E3SM are described in (*84*). Sea surface temperature, sea ice, and other input fields were prescribed as described in (*80*), but using a perpetual year 2010 to represent nominal near-present-day conditions.

Aerosol microphysics is simulated using the four-mode version of the Modal Aerosol Module (MAM4; (*85, 86*)). The MAM4 module treats the major aerosol species, including sulfate, black carbon, mineral dust, sea salt aerosol, primary organic aerosol, secondary organic aerosol, and marine organic aerosol (MOA). It also simulates aerosol microphysics and loss processes, including condensational growth, coagulation, and wet and dry deposition.

Natural wind-driven dust emissions in E3SMv1 are calculated using the Dust Entrainment and Deposition model (*87*). Emitted dust follows a prescribed size distribution, with emissions varying as a function of surface wind speed, friction velocity, and a prescribed soil erodibility index.

Sea salt emission fluxes are simulated as a function of near-surface wind speed and prescribed sea surface temperature, with a fixed emission size distribution. Sea salt emissions follow (*88*) from 20 nm—2.5 μm, and (*89*) from 2.5—10 μm. MOA emissions are simulated using the OCEANFILMS parameterization (*90*). Emitted MOA is assumed to be internally mixed with sea salt, and the relevant surface area for use in the M18 sea spray INP parameterization is assumed to be the surface area of these internally-mixed organic-salt particles. However, the impacts of MOA on E3SM-simulated sea spray are minor in this study, and are generally minor in the North Pacific and coastal California (*90*), despite having important impacts elsewhere.

The instantaneous dust and sea spray mass emissions simulated by E3SM were saved at 3-hourly intervals for use in the source-receptor analysis. Emissions were assumed to follow the fixed size distributions of the respective emissions parameterizations. Additionally, aerosol fields simulated at the nearest neighboring grid point to the observation site were archived at high frequency for comparison with observed aerosol and INPs.

Deriving source-receptor footprints using Lagrangian dispersion modeling

Source-receptor influence footprints (hereafter S-R footprints) (*41*) are commonly used in air quality modeling to relate the concentration of an atmospheric constituent at one location to the potential influence of source regions on the observed concentration. Source-receptor analysis is appropriate for relating emission functions to observations in situations where the sources are regionally widespread, observations are made at a single point, and relevant atmospheric transformation and removal processes can be adequately represented by the Lagrangian model.

We use the Lagrangian dispersion models FLEXPART v 10.4 (*40*) and FLEXPART-WRF (*91*) to derive S-R footprints for our sampling periods. A full description of the model(s) is beyond

the scope of this study, but in brief, FLEXPART(-WRF) uses meteorological input data to drive the transport of inert parcels through time and space. These two models have the same computational framework but use different input data to drive the simulations. We ran the FLEXPART simulations using the National Center for Environmental Prediction (NCEP) Climate Forecast System Version 2 (https://rda.ucar.edu/datasets/ds094.1/) to drive global simulations. We ran the FLEXPART-WRF simulations using a WRF simulation centered over the Western United States (described below). Parcel advection is driven by mean winds from the meteorological data, with a turbulent diffusion component that is parameterized based upon its position in the atmosphere. Each parcel is assigned an initial aerosol mass; mass can subsequently be removed by dry and wet deposition. Parcels are also assigned physical properties, including aerosol size and density, which dictate their susceptibility to deposition processes.

To derive the S-R footprints, we ran 10-day simulations backward in time. FLEXPART(-WRF) simulations were conducted for the impinger sampling (98 in total) and the PCVI sampling periods (7 in total). We released 10,000 parcels, evenly distributed in time over the course of the given sampling period, and tracked them backward in time for 10 days. S-R footprints were calculated at 15-minute intervals, at 1 degree resolution, assuming an envelope height of 300 m. Figures S8 and S9 show the average S-R footprints for FLEXPART simulations run using NCEP and WRF meteorology respectively.

Regional scale modeling for input into Lagrangian modeling

The WRF model version 3.9.1 (ARW, (*92*)) is used to conduct the regional atmospheric simulations which provide input data for the Lagrangian simulations performed using FLEXPART-WRF. The domain (Fig. S10) encompasses part of the western U.S. and adjacent Pacific Ocean with its center at Bodega Bay. The domain uses a horizontal grid spacing of 4 km (1000 x 1000 grid points) and a stretched vertical coordinate with 60 levels up to the model top at 100 hPa. The model simulations use the Thompson microphysics parameterization (*93*), Mellor-Yamada-Nakanishi Niino (MYNN) boundary layer parameterization (*94*), Mellor-Yamada-Janjic surface layer parameterization (*95*), Unified Noah land-surface parameterization (*96*), and the RRTMG longwave and shortwave radiation parameterization (*97*). The NCEP FNL operational model global tropospheric analysis with 1° grid spacing is used to initialize the model's atmosphere and soil variables.

The WRF simulations are constrained by coupling with a three-dimensional variational (3DVar) assimilation scheme provided in the Community Gridpoint Statistical Interpolation (GSI, (*98*). We assimilated observations from the NCEP Global Upper Air and Surface Weather Observations dataset (http://rda.ucar.edu/datasets/ds337.0/) following a previously established methodology (*99*). These observations include, but are not limited to, radiosonde profiles, surface meteorology, aircraft, and ship measurements. The assimilation cycle assimilation was carried out every 12 hours from January 6 through March 11 of 2015. Model variables such as zonal and meridional winds, specific humidity, temperature, and pressure are updated at 00 and 12 UTC based on analyzed increments, and the updated analysis at each time is used to initialize the subsequent 12-hour forecast.

Particle source functions for predicting INPs

Particle source functions during the CalWater-2015 study were generated for the relevant INP sources: dust, SSA, bacteria, and fungal spores. The instantaneous emissions of dust and SSA were simulated by E3SM, and saved at 3-hourly intervals (see section on aerosol modeling in E3SM). Particle surface areas were calculated by assuming a spherical geometry with a diameter of 2 μm for bacteria-bearing particles and 4 μm for fungal spores, and assuming a geometric standard

deviation of 1.5 for both species. Bacteria emission fluxes were taken from a time-independent emission map (*42*). For fungal spore emissions, we follow a recently-developed emissions model (*43*), wherein emissions are parameterized as a function of specific humidity at 2m (q_{2m}), the leaf area index (LAI), and the friction velocity (u^*). We used hourly North American Mesoscale Forecast System (NAM) Analysis data for q_{2m} and u^*, and the 4-day LAI observations from MODIS (*100*). All data was down-scaled to 1° x 1° resolution prior to the calculation of fungal spore emission fluxes.

All INP concentrations were calculated using the active site density (n_s), which is a deterministic (i.e. time-independent) surface area based metric of IN-activity. INP concentrations for dust were calculated using the N12 parameterization (*27*). INP concentrations for SSA were calculated using a parameterization developed using ambient measurements at Mace Head Observatory in Ireland (*28*). INP concentrations for bacteria and fungal spores were calculated using empirical parameterizations fit from ambient measurements (*45*).

Alignment of ice nucleation measurements

Bulk immersion mode ice nucleating particle (INP) concentrations were measured using two instruments: (1) the North Carolina State University (NCSU) cold stage (CS) and (2) the Colorado State University (CSU) ice spectrometer (IS). The two instruments both sampled ambient air but using different collection methods. The NCSU CS used impinger samplers (SKC Inc. BioSampler®) to sample ambient air (*33*) for approximately four hour sampling periods. The CSU IS used open-faced filters to sample ambient aerosol, with sampling periods lasting from 4-38 hours, but most frequently around 15-16 hours. The higher time resolution of the impingers allowed us to collect 98 samples, compared to the 56 from the filters. Thus the impingers were able to observe greater variability in both INP concentrations and composition, and it is advantageous to use in our analysis. However, the impingers were located approximately 10 m away from the sampling trailers containing the other instruments, with a difference in sampling height of 3-4 m. The filter unit was located on top of the sampling trailer, next to the aerosol inlet, making it directly comparable. We observed a 5-fold difference in the concentrations measured by the two instruments over the course of the study (Fig. S11). We note that we are unaware of any studies have shown significant spatial heterogeneity in INP concentrations over such short distances. We also found that despite the difference in sampling durations, the key particle composition metrics used in our study had the same concentration distributions for both sampling methods (Fig. S12) and therefore we look to other explanations for the difference in INP concentrations between the two datasets.

We find it plausible that the different aerosol collection methods could have contributed to some of the difference in INP concentrations as bioaerosol may be especially sensitive to the sample collection methodology. Compared to filter sampling, impingers exert less physiological stress on cells, allowing them to more effectively sample *culturable* bioaerosol (*101*). The loss in viability associated with filter sampling also increases with sampling duration (*102*), which may be pertinent here due to the long sampling times associated with the filter collections. While we are not aware of any studies that directly link a loss in viability with decreased IN activity, it is plausible that viability indirectly reflects the structural integrity of bioparticles, and which may affect their IN-activity. However, direct comparisons between INP measurements from samples collected with filters and those collected with impingers found that they agreed broadly, with measurements within one order of magnitude (*103, 104*). This agreement varied depending on the case, and the more important question is whether the techniques systematically disagree over a long time period. Presumably, if there was no bias to either collection method then these

differences would even out over the course of the study. However, as we do see bias in our results we cannot eliminate this possibility.

Finally, we note that intercomparison efforts assessing the replicability of different ice counters have generally found that the ice spectrometer and cold stage to broadly agree (*103–105*), with measurements generally being within an order of magnitude of each other. Similar to the aerosol collection method, the important question is whether there is a systematic disagreement between the instrument performance. If there is a bias with the temperature measurement for either instrument then this could help explain the difference in INP concentrations. Previous work has noted a small bias between the IS and CS for samples with temporal overlap, which averaged out to a difference of roughly 2-3x. However, the sampling there took place over a much shorter duration than this study and it is not clear if the bias would have been observed when sampling over a longer duration. Therefore, we cannot rule out systematic bias due to differences in instrument performance.

As we cannot rule out systematic bias, we have elected to downscale the CS measurements by a factor of 5 to bring them into alignment with the IS measurements. We chose this approach because it provides a more conservative measure of INP concentrations while retaining temporal resolution. We tested the implications of this choice on our findings by repeating all analyses presented in this paper using the IS measurements in place of the CS measurements. The major conclusions of the study were insensitive to the choice of dataset. Specifically, bioaerosols remain the dominant source of warm-temperature INPs (Fig. S13) and the dominant source of prediction error regardless of which INP measurement is used.

Metrics to evaluate predicted INP concentrations.

We use two metrics to assess model predictive skill. The first is the modified normalized mean bias (MNMB), which describes the average difference between predictions and measurements. It ranges from -2 to 2, with 0 indicating perfect prediction. The MNMB is calculated by the following:

$$MNMB = \frac{2}{n}\sum_{i}\frac{P_i - M_i}{P_i + M_i}$$

where n is the number of samples, P_i is the predicted value for sample i, and M_i is the measured value for sample i. The second skill score we use is the fractional gross error (FGE), which describes the total average absolute error. The FGE ranges from 0 to 2, with 0 indicating perfect agreement between predictions and measurements. The FGE is given by

$$FGE = \frac{2}{n}\sum_{i}\left|\frac{P_i - M_i}{P_i + M_i}\right|$$

where n is the number of samples, P_i is the predicted value for sample i, and M_i is the measured value for sample i. These metrics have been recommended for evaluating predictions of atmospheric composition measurements because they are symmetrical to relative over- and under-prediction (*106*).

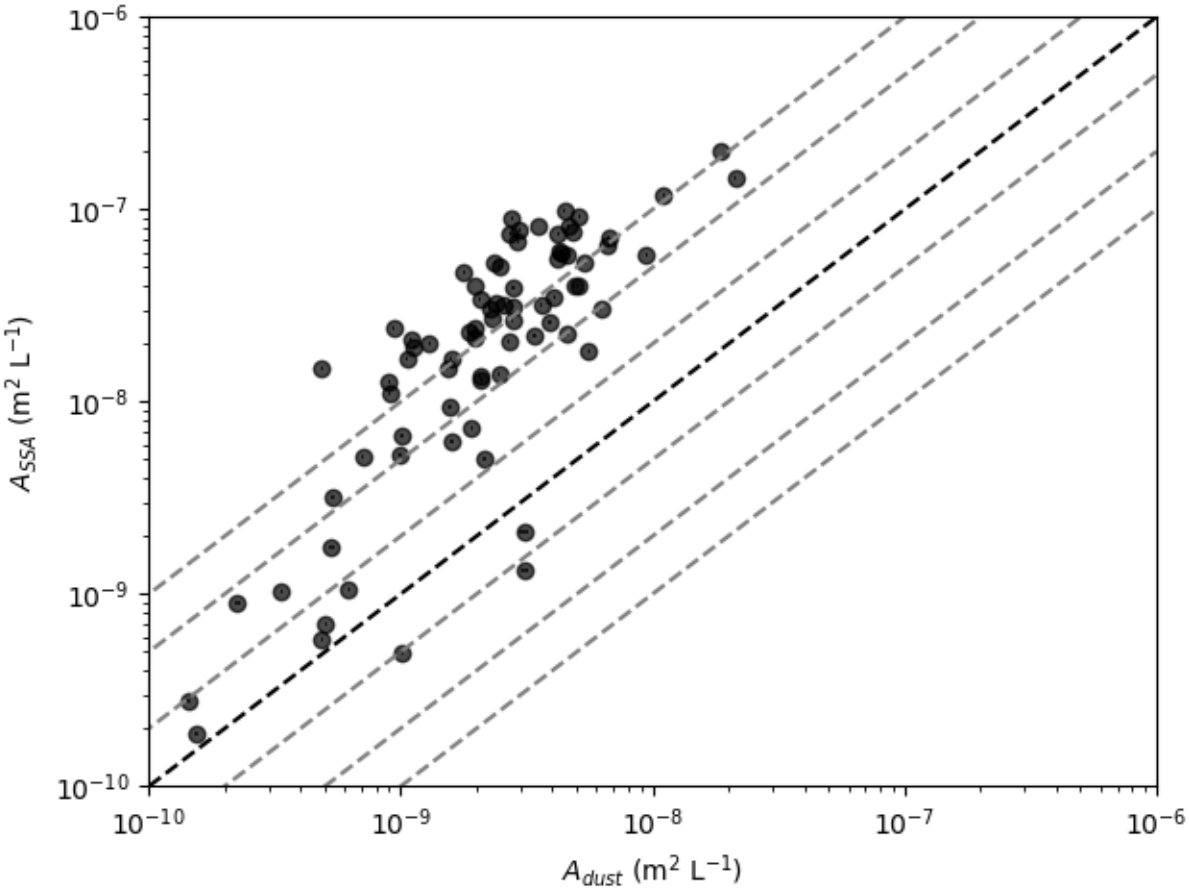

Fig. S1.

Scatter plot of the measured surface area concentration for sea spray aerosol (A_{SSA}) vs the measured surface area concentration for dust particles (A_{dust}). Values are calculated for the INP sampling periods. Dashed black lines shows the 1:1 line, while the grey dashed lines show the 10:1, 5:1, 2:1, 1:2, 1:5, and 1:10 lines.

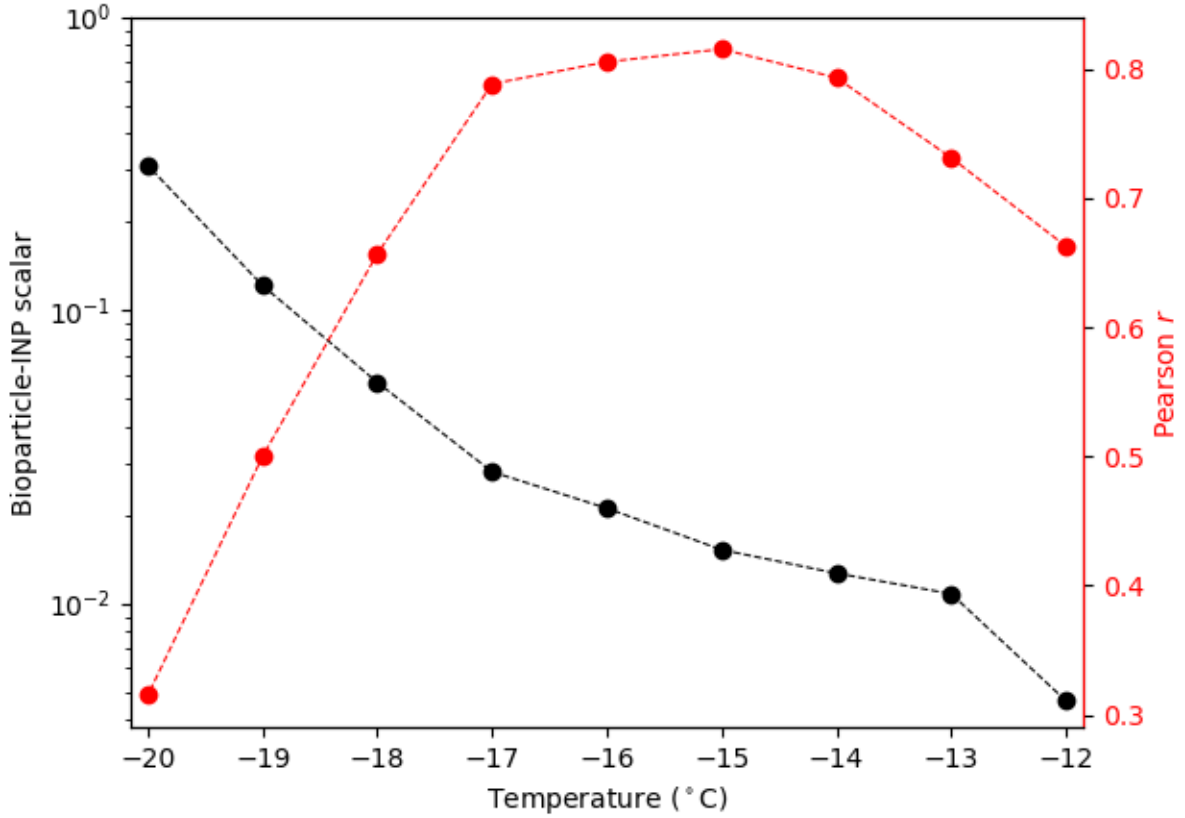

Fig. S2.

Scatter plot of bioparticle-INP scalar vs temperature (green). The Pearson *r* correlation coefficient is also shown (red).

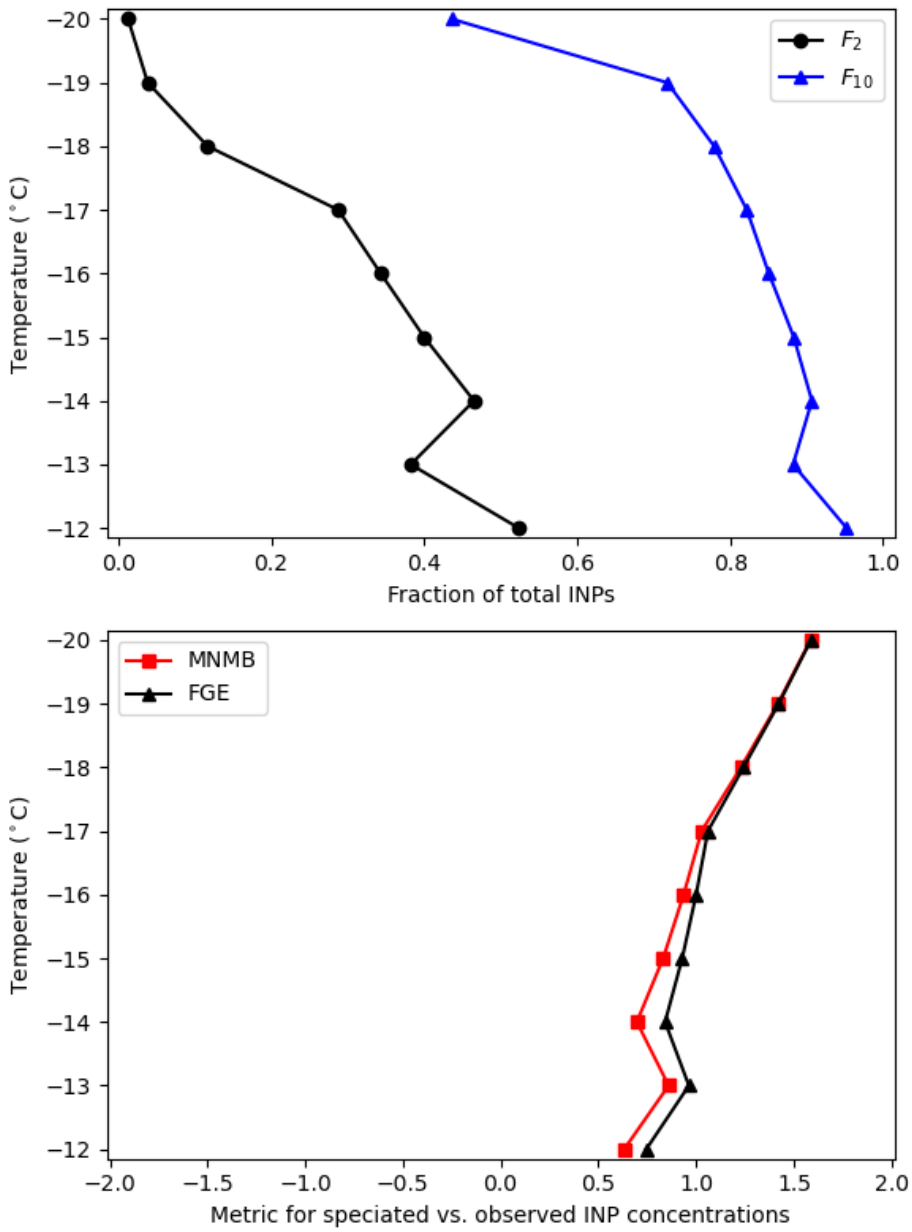

Fig. S3.

Metrics for comparing total speciated INPs vs total INP concentrations. Panel A shows the fraction of measurement periods where predicted INP concentrations fall within a factor of 2 (F_2; black)$ and within a factor of 10 (F_{10}; blue) of observed INP concentration, as a function of temperature. Panel B shows the modified normalized mean bias (MNMB; red) and fraction gross error (FGE; green).

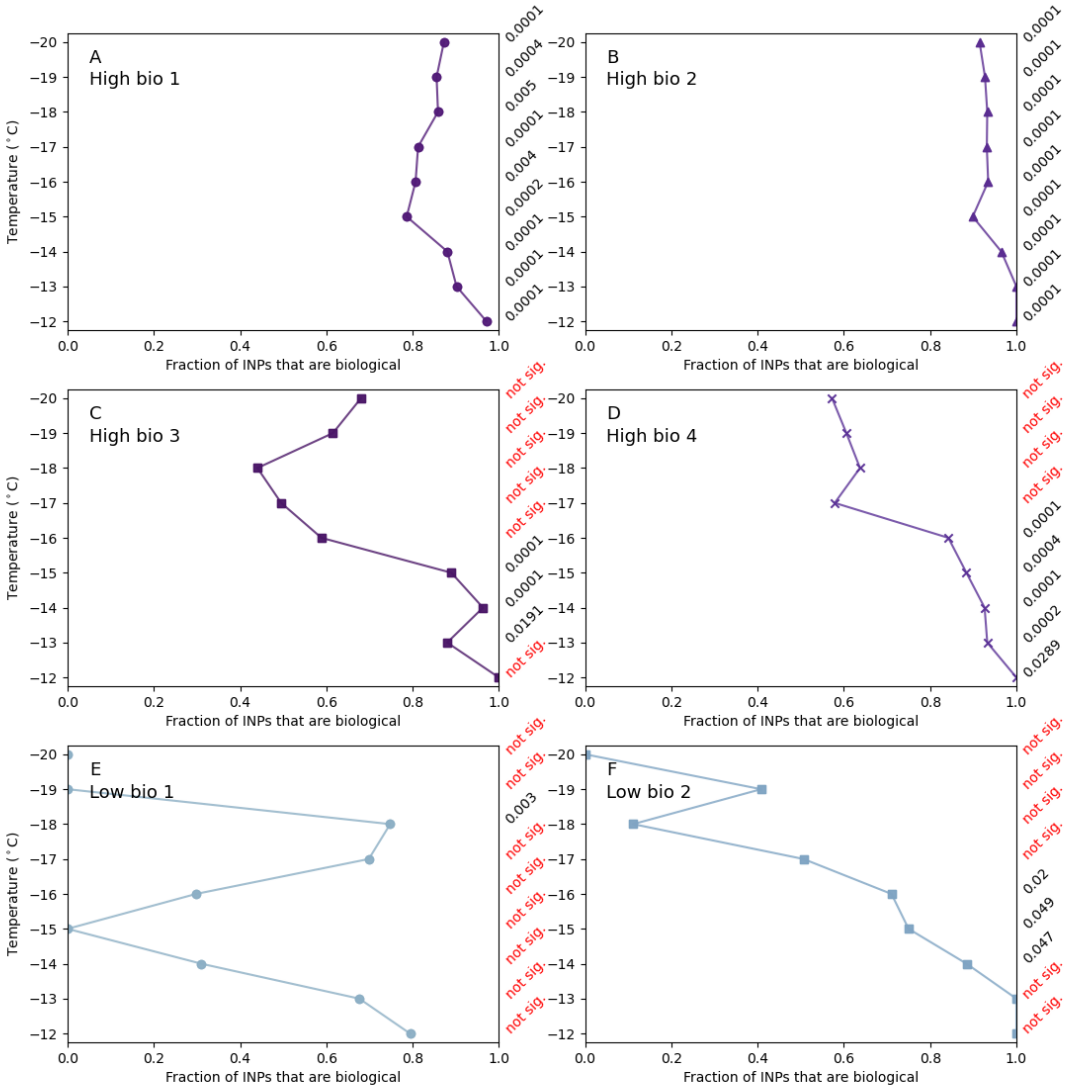

Fig. S4.

Fraction of INPs determined to be biological from the heat treatment of samples measured by the ice spectrometer. Panels A-D show samples with high bioparticle concentrations, while panels E and F show samples with low bioparticle concentrations. P-values calculated using Fisher's Exact Test are displayed on the right axis.

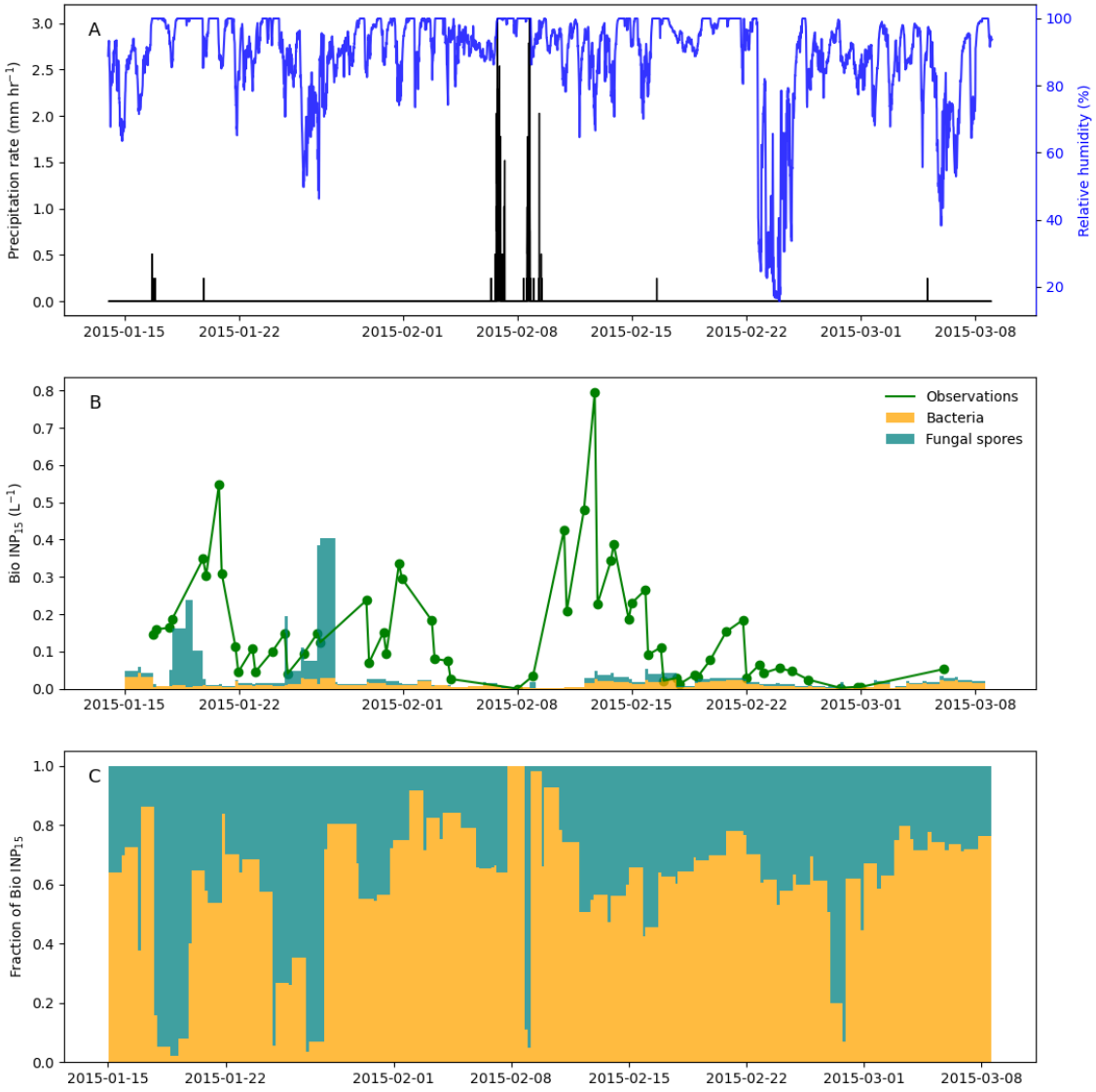

Fig. S5.

Time series for meteorological measurements and observed and predicted bio-INPs. **(A)** Top panel shows the timeseries for the precipitation rate (black) and the relative humidity (blue). Middle panel shows. (B) Middle panel shows the timeseries of observed bioparticle (Bio) ice nucleating particle (INP) concentrations active at -15 °C (Bio $INP_{-15;}$ green) along with the predicted INP concentrations from bacteria (orange) and fungal spores (teal). **(C)** Bottom panel shows the fraction of predicted Bio INP_{-15} coming from bacteria and fungal spores.

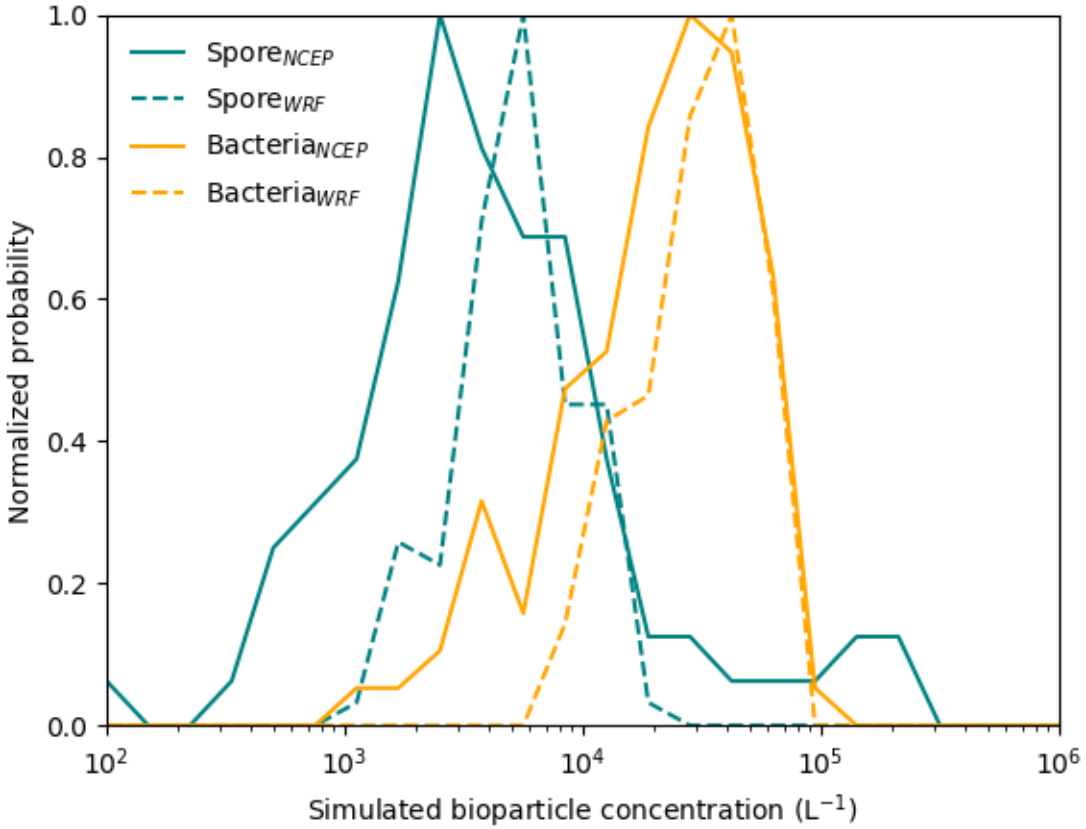

Fig. S6.

Normalized probability distributions for simulated fungal spore (green trace) and bacteria (yellow trace) concentrations. The continuous line shows particle concentrations for particles simulated using NCEP input data, while the dashed line shows denotes lines simulated using WRF input data.

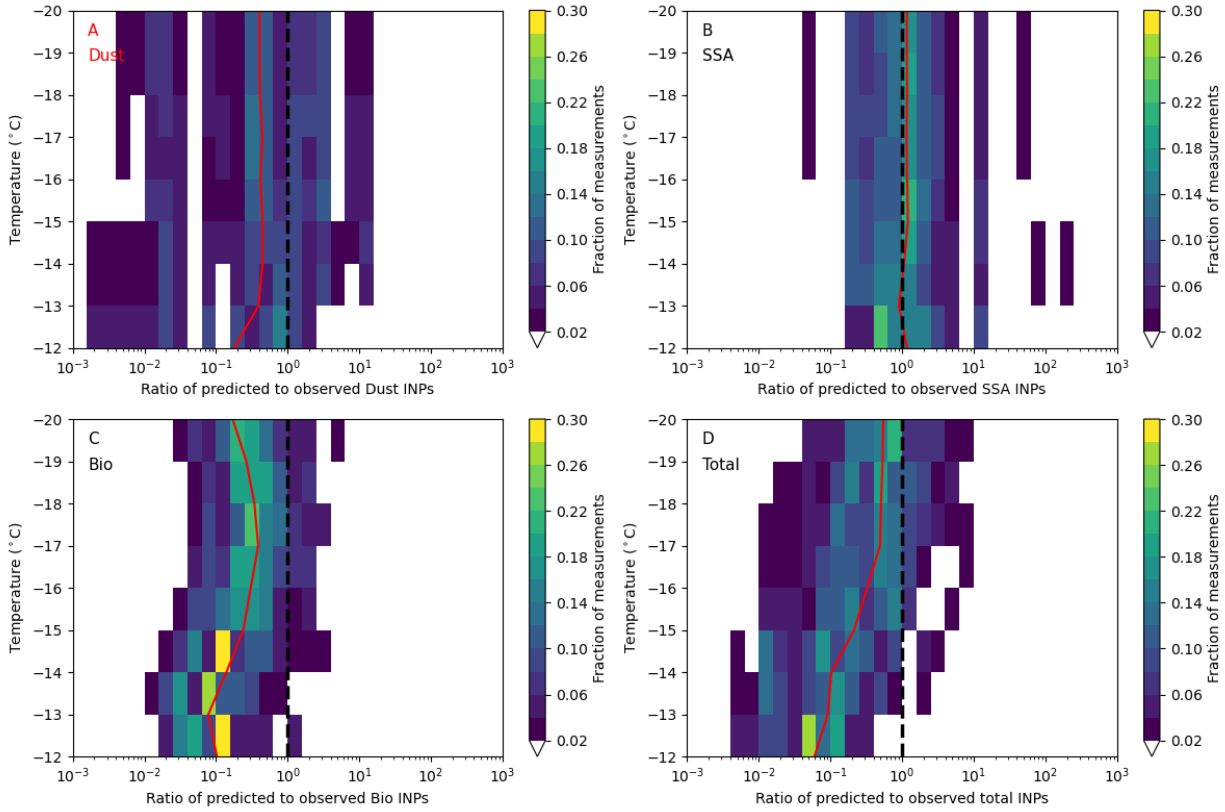

Fig. S7.

Heat maps of the ratios of predicted to observed INPs as a function of temperature for **(A)** Dust, **(B)** SSA, **(C)** Bio, and **(D)** total INPs. Red lines show the median values for each temperature. Dashed black lines show the 1:1 line where predicted INPs agree with observed INPs. INP concentrations were predicted using source-receptor footprints derived from the simulations driven by limited-area simulations.

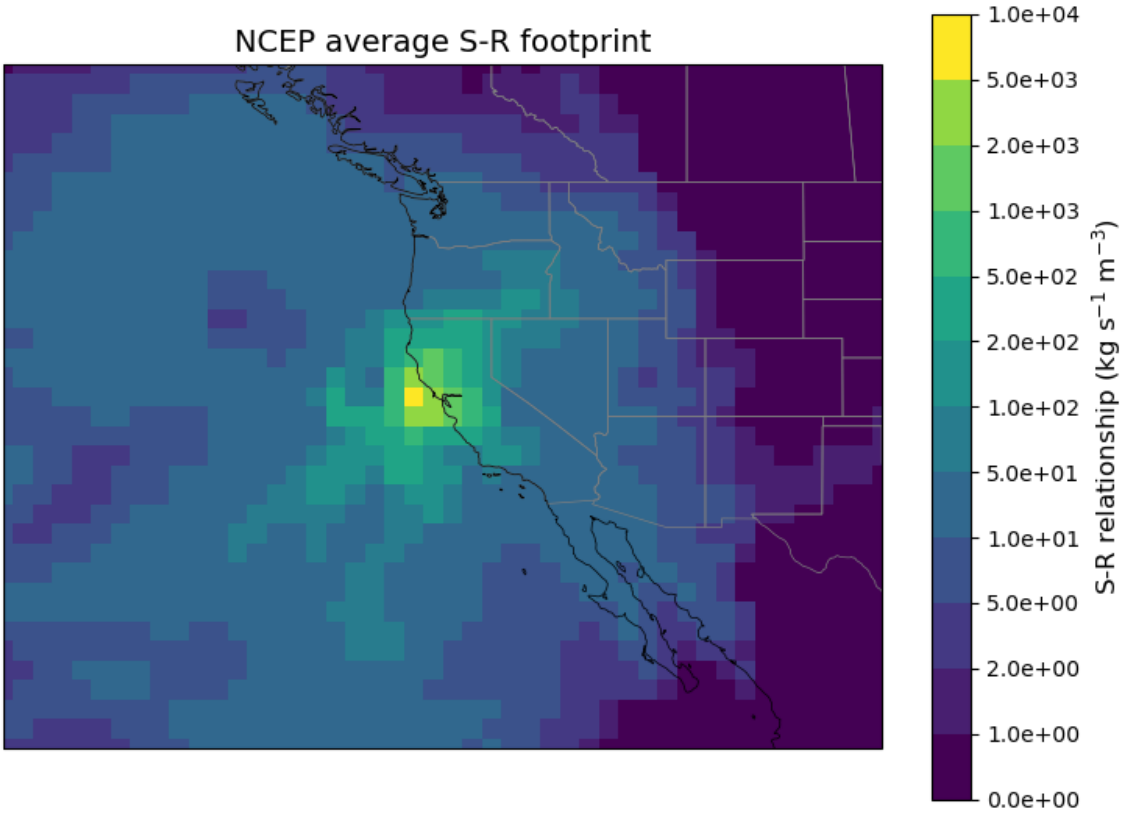

Figure S8.
Average S-R footprint from all FLEXPART simulations run using NCEP meteorology.

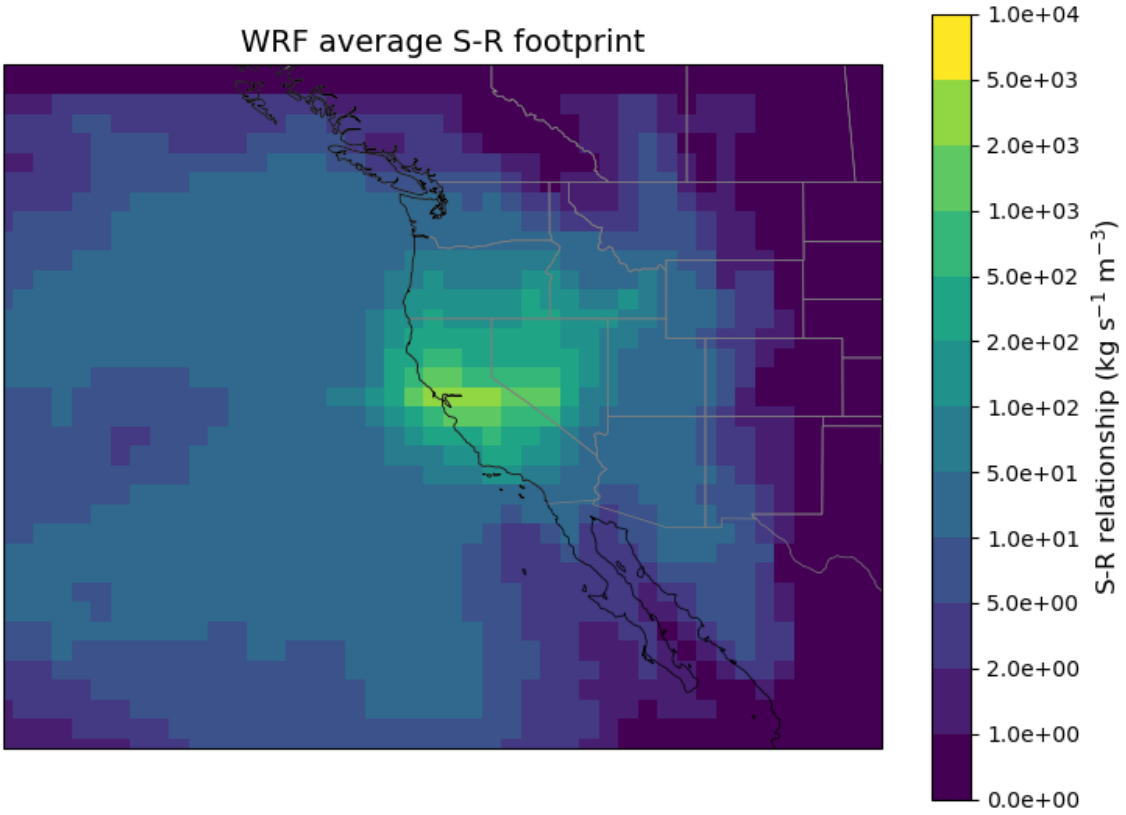

Figure S9.
Average S-R footprint from all FLEXPART simulations run using WRF output meteorology.

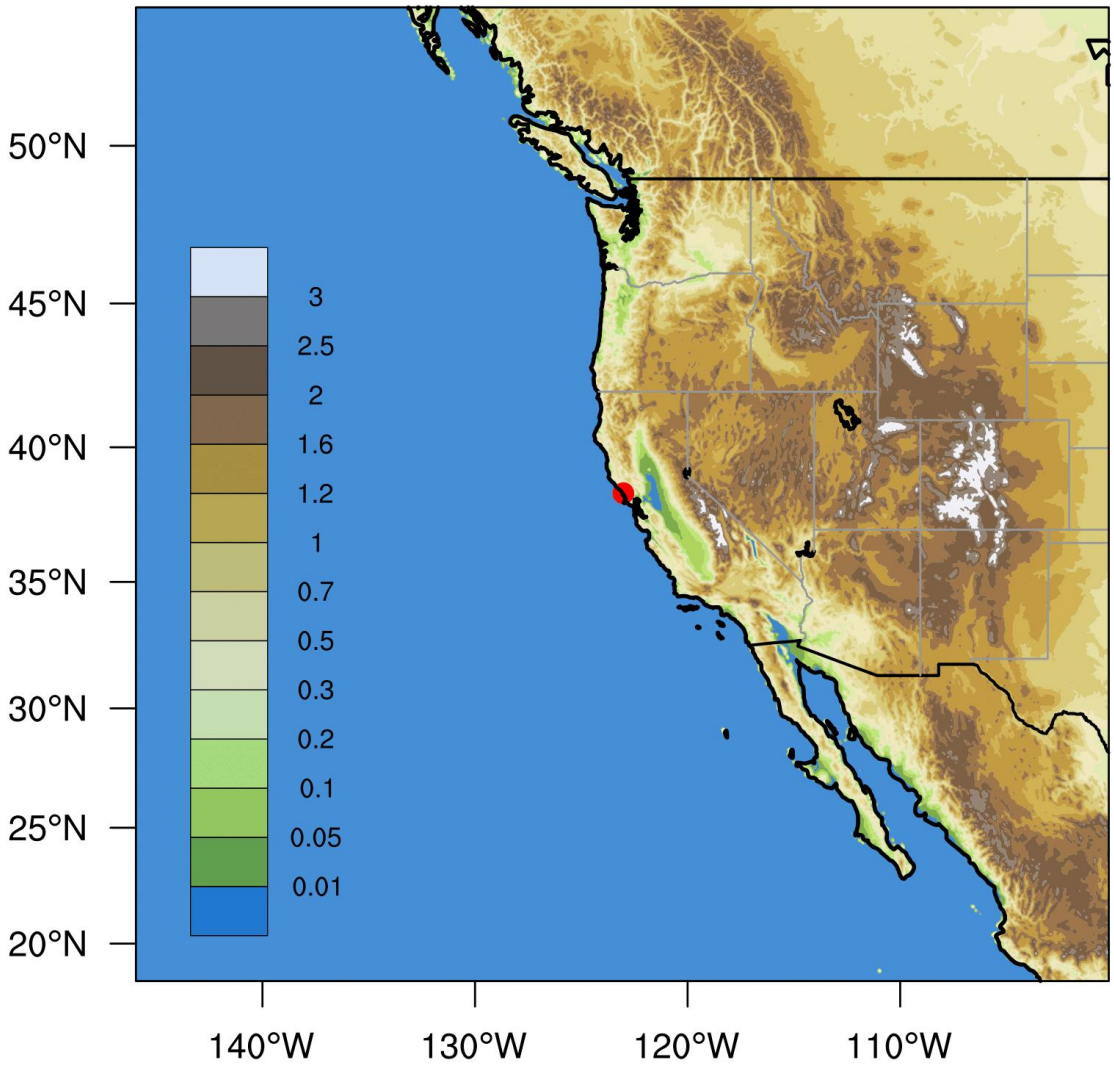

Fig. S10.
Domain of the WRF simulations. Shading indicates the terrain height.

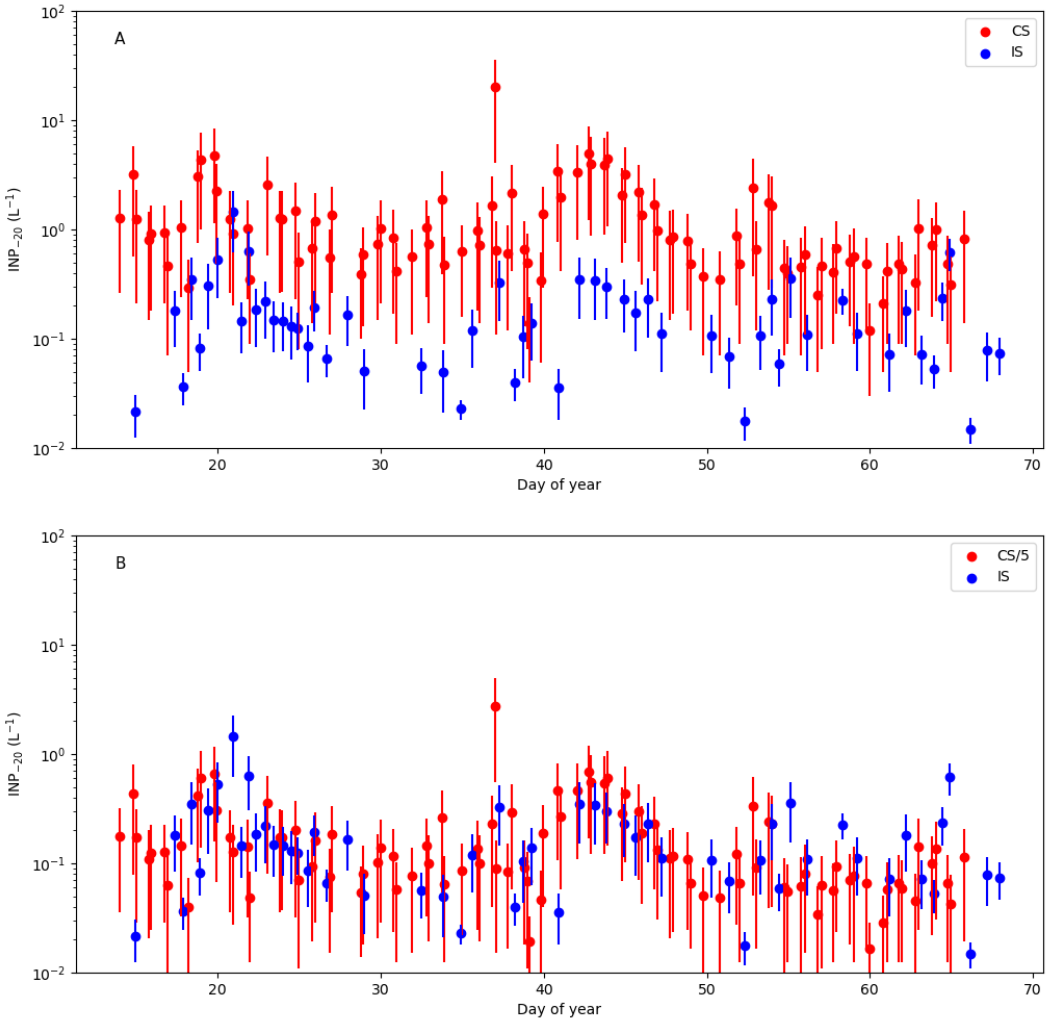

Fig. S11.

INP$_{-20}$ concentrations from the NCSU cold stage (CS; red circles) and the CSU ice spectrometer (IS; blue circles). Top plot shows the unscaled concentrations for both samples, while the bottom plot shows the same data except that the CS measurements are scaled down by a factor of five.

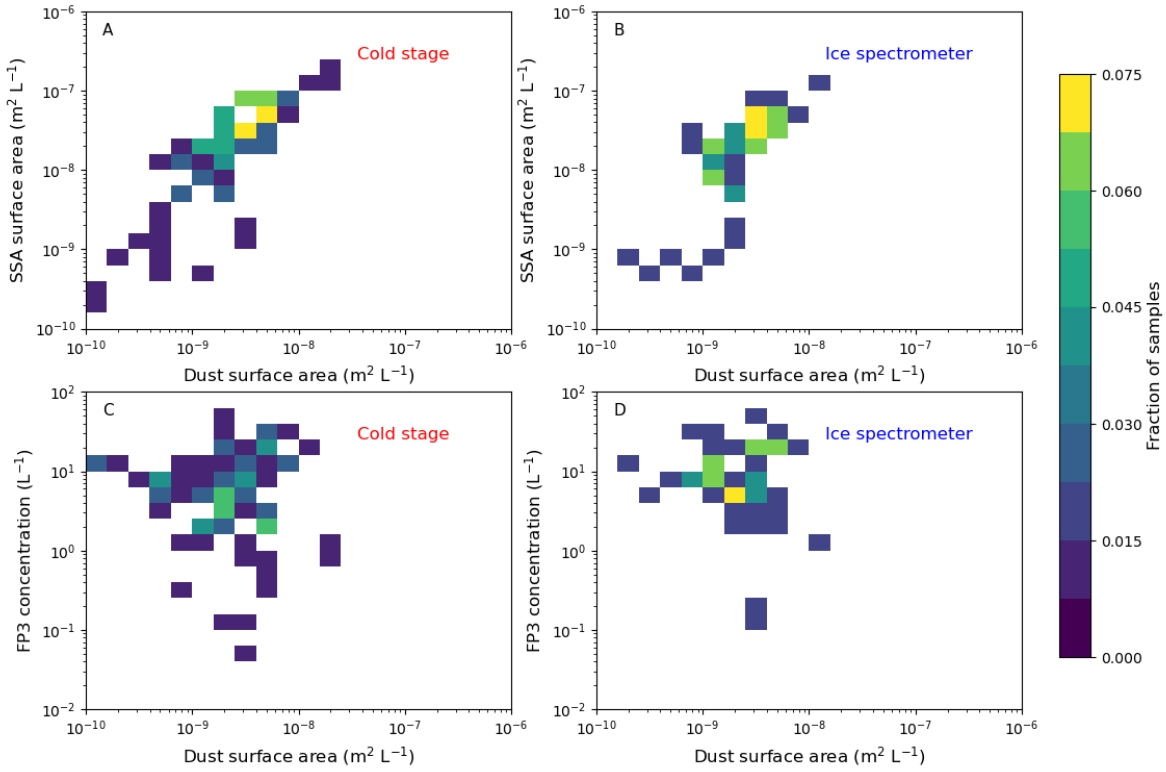

Fig. S12.

Heat maps of the distribution of particle composition measurements for INP sampling periods. Panel A shows SSA surface area concentrations vs dust surface area concentrations for the time periods corresponding to the cold stage impinger measurements. Panel B shows SSA surface area concentrations vs dust surface area concentrations for the time periods corresponding to the ice spectrometer filter measurements. Panel C shows the concentration of FP3 particles measured by the WIBS vs dust surface area concentrations for the time periods corresponding to the cold stage impinger measurements. Panel D shows the concentration of FP3 particles measured by the WIBS vs dust surface area concentrations for the time periods corresponding to the cold stage impinger measurements.

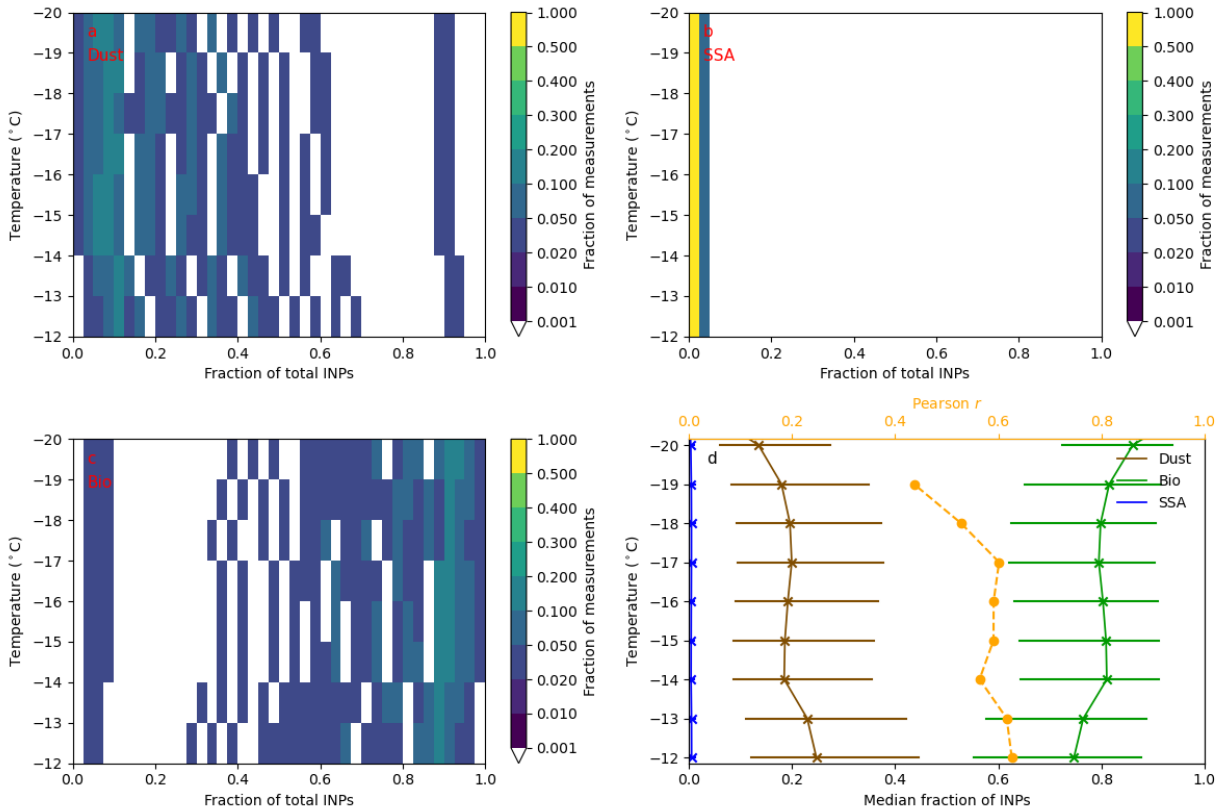

Fig. S13.
Heat maps of the fraction of speciated INPs as a function of temperature. Speciated INPs are derived from the ice spectrometer measurements. Panels show the fraction for **(A)** Dust, **(B)** SSA, and **(C)** Bio (bio-INPs). Figure shading shows the fraction of INP samples between the upper and lower bounds of that bin. Panel **(D)** shows the median estimated fraction of INPs from dust (brown), SSA (blue), and Bio (green). The horizontal bars show the interquartile ranges. Also shown is the Pearson correlation coefficient *r* for the fit between the total speciated INPs and measured INPs.

REFERENCES AND NOTES

1. P. J. DeMott, A. J. Prenni, X. Liu, S. M. Kreidenweis, M. D. Petters, C. H. Twohy, M. Richardson, T. Eidhammer, D. Rogers, Predicting global atmospheric ice nuclei distributions and their impacts on climate. *Proc. Natl. Acad. Sci. U.S.A.* **107**, 11217–11222 (2010).

2. Y.-S. Choi, R. S. Lindzen, C.-H. Ho, J. Kim, Space observations of cold-cloud phase change. *Proc. Natl. Acad. Sci. U.S.A.* **107**, 11211–11216 (2010).

3. J. Vergara-Temprado, A. K. Miltenberger, K. Furtado, D. P. Grosvenor, B. J. Shipway, A. A. Hill, J. M. Wilkinson, P. R. Field, B. J. Murray, K. S. Carslaw, Strong control of Southern Ocean cloud reflectivity by ice-nucleating particles. *Proc. Natl. Acad. Sci. U.S.A.* **115**, 2687–2692 (2018).

4. R. E. Hawker, A. K. Miltenberger, J. M. Wilkinson, A. A. Hill, B. J. Shipway, Z. Cui, R. J. Cotton, K. S. Carslaw, P. R. Field, B. J. Murray, The temperature dependence of ice-nucleating particle concentrations affects the radiative properties of tropical convective cloud systems. *Atmos. Chem. Phys.* **21**, 5439–5461 (2021).

5. J. Fan, L. R. Leung, D. Rosenfeld, P. J. Demott, Effects of cloud condensation nuclei and ice nucleating particles on precipitation processes and supercooled liquid in mixed-phase orographic clouds. *Atmos. Chem. Phys.* **17**, 1017–1035 (2017).

6. I. Tan, D. Barahona, Q. Coopman, Potential link between ice nucleation and climate model spread in arctic amplification. *Geophys. Res. Lett.* **49**, e2021GL097373 (2022).

7. L. B. Hande, C. Hoose, Partitioning the primary ice formation modes in large eddy simulations of mixed-phase clouds. *Atmos. Chem. Phys.* **17**, 14105–14118 (2017).

8. D. A. Knopf, K. R. Barry, T. A. Brubaker, L. G. Jahl, K. A. Jankowski, J. Li, Y. Lu, L. W. Monroe, K. A. Moore, F. A. Rivera-Adorno, K. A. Sauceda, Y. Shi, J. M. Tomlin, H. S. K. Vepuri, P. Wang, N. N. Lata, E. J. T. Levin, J. M. Creamean, T. C. J. Hill, S. China, P. A. Alpert, R. C. Moffet, N. Hiranuma, R. C. Sullivan, A. M. Fridlind, M. West, N. Riemer, A. Laskin, P. J. DeMott, X. Liu, Aerosol–ice formation closure: A southern great plains field campaign. *Bull. Am. Meteorol. Soc.* **102**, E1952–E1971 (2021).

9. S. M. Burrows, C. S. McCluskey, G. Cornwell, I. Steinke, K. Zhang, B. Zhao, M. Zawadowicz, A. Raman, G. Kulkarni, S. China, A. Zelenyuk, P. J. DeMott, Ice-nucleating particles that impact clouds and climate: Observational and modeling research needs. *Rev. Geophys.* **60**, e2021RG000745 (2022).

10. B. J. Murray, D. O'Sullivan, J. D. Atkinson, M. E. Webb, Ice nucleation by particles immersed in supercooled cloud droplets. *Chem. Soc. Rev.* **41**, 6519–6554 (2012).

11. Z. A. Kanji, L. A. Ladino, H. Wex, Y. Boose, M. Burkert-Kohn, D. J. Cziczo, M. Krämer, Overview of ice nucleating particles. *Meteorol. Monogr.* **58**, 1.1–1.33 (2017).

12. S. Huang, W. Hu, J. Chen, Z. Wu, D. Zhang, P. Fu, Overview of biological ice nucleating particles in the atmosphere. *Environ. Int.* **146**, 106197 (2021).

13. D. V. Spracklen, C. L. Heald, The contribution of fungal spores and bacteria to regional and global aerosol number and ice nucleation immersion freezing rates. *Atmos. Chem. Phys.* **14**, 9051–9059 (2014).

14. A. Korolev, T. Leisner, Review of experimental studies of secondary ice production. *Atmos. Chem. Phys.* **20**, 11767–11797 (2020).

15. A. Takeishi, T. Storelvmo, A study of enhanced heterogeneous ice nucleation in simulated deep convective clouds observed during DC3. *J. Geophys. Res. Atmos*. **123**, 13396–13420 (2018).

16. J. Wieder, N. Ihn, C. Mignani, M. Haarig, J. Bühl, P. Seifert, R. Engelmann, F. Ramelli, Z. A. Kanji, U. Lohmann, J. Henneberger, Retrieving ice-nucleating particle concentration and ice multiplication factors using active remote sensing validated by in situ observations. *Atmos. Chem. Phys.* **22**, 9767–9797 (2022).

17. T. C. J. Hill, P. J. DeMott, Y. Tobo, J. Fröhlich-Nowoisky, B. F. Moffett, G. D. Franc, S. M. Kreidenweis, Sources of organic ice nucleating particles in soils. *Atmos. Chem. Phys.* **16**, 7195–7211 (2016).

18. M. I. Daily, M. D. Tarn, T. F. Whale, B. J. Murray, An evaluation of the heat test for the ice-nucleating ability of minerals and biological material. *Atmos. Meas. Tech.* **15**, 2635–2665 (2022).

19. R. H. Mason, M. Si, J. Li, C. Chou, R. Dickie, D. Toom-Sauntry, C. Pöhlker, J. D. Yakobi-Hancock, L. A. Ladino, K. Jones, W. R. Leaitch, C. L. Schiller, J. P. D. Abbatt, J. A. Huffman, A. K. Bertram, Ice nucleating particles at a coastal marine boundary layer site: Correlations with aerosol type and meteorological conditions. *Atmos. Chem. Phys.* **15**, 12547–12566 (2015).

20. G. C. Cornwell, C. S. McCluskey, E. J. T. Levin, K. J. Suski, P. J. DeMott, S. M. Kreidenweis, K. A. Prather, Direct online mass spectrometry measurements of ice nucleating particles at a california coastal site. *J. Geophys. Res. Atmos*. **124**, 12157–12172 (2019).

21. Z. A. Kanji, R. C. Sullivan, M. Niemand, P. J. DeMott, A. J. Prenni, C. Chou, H. Saathoff, O. Möhler, Heterogeneous ice nucleation properties of natural desert dust particles coated with a surrogate of secondary organic aerosol. *Atmos. Chem. Phys.* **19**, 5091–5110 (2019).

22. G. P. Schill, P. J. DeMott, E. W. Emerson, A. M. C. Rauker, J. K. Kodros, K. J. Suski, T. C. Hill, E. J. Levin, J. R. Pierce, D. K. Farmer, The contribution of black carbon to global ice nucleating particle concentrations relevant to mixed-phase clouds. *Proc. Natl. Acad. Sci. U.S.A.* **117**, 22705–22711 (2020).

23. S. Kasparoglu, R. Perkins, P. J. Ziemann, P. J. DeMott, S. M. Kreidenweis, Z. Finewax, B. L. Deming, M. P. DeVault, M. D. Petters, Experimental determination of the relationship between organic aerosol viscosity and ice nucleation at upper free tropospheric conditions. *J. Geophys. Res. Atmos.* **127**, e2021JD036296 (2022).

24. C. Wu, Z. Lin, X. Liu, The global dust cycle and uncertainty in CMIP5 (coupled model intercomparison project phase 5) models. *Atmos. Chem. Phys.* **20**, 10401–10425 (2020).

25. B. Testa, T. C. J. Hill, N. A. Marsden, K. R. Barry, C. C. Hume, Q. Bian, J. Uetake, H. Hare, R. J. Perkins, O. Möhler, S. M. Kreidenweis, P. J. DeMott, Ice nucleating particle connections to regional argentinian land surface emissions and weather during the cloud, aerosol, and complex terrain interactions experiment. *J. Geophys. Res. Atmos.* **126**, e2021JD035186 (2022).

26. E. Gard, J. E. Mayer, B. D. Morrical, T. Dienes, D. P. Fergenson, K. A. Prather, Real-time analysis of individual atmospheric aerosol particles: Design and performance of a portable ATOFMS. *Anal. Chem.* **69**, 4083–4091 (1997).

27. M. Niemand, O. Möhler, B. Vogel, H. Vogel, C. Hoose, P. Connolly, H. Klein, H. Bingemer, P. DeMott, J. Skrotzki, T. Leisner, A particle-surface-area-based parameterization of immersion freezing on desert dust particles. *J. Atmos. Sci.* **69**, 3077–3092 (2012).

28. C. S. McCluskey, J. Ovadnevaite, M. Rinaldi, J. Atkinson, F. Belosi, D. Ceburnis, S. Marullo, T. C. J. Hill, U. Lohmann, Z. A. Kanji, C. O'Dowd, S. M. Kreidenweis, P. J. DeMott, Marine and terrestrial organic ice-nucleating particles in pristine marine to continentally influenced northeast atlantic air masses. *J. Geophys. Res. Atmos*. **123**, 6196–6212 (2018).

29. K. D. Froyd, D. M. Murphy, C. A. Brock, P. Campuzano-Jost, J. E. Dibb, J.-L. Jimenez, A. Kupc, A. M. Middlebrook, G. P. Schill, K. L. Thornhill, C. J. Williamson, J. C. Wilson, L. D. Ziemba, A new method to quantify mineral dust and other aerosol species from aircraft platforms using single-particle mass spectrometry. *Atmos. Meas. Tech.* **12**, 6209–6239 (2019).

30. G. C. Cornwell, C. S. McCluskey, P. J. DeMott, K. A. Prather, S. M. Burrows, Development of heterogeneous ice nucleation rate coefficient parameterizations from ambient measurements. *Geophys. Res. Lett.* **48**, e2021GL095359 (2021).

31. J. Vergara-Temprado, B. J. Murray, T. W. Wilson, D. O'Sullivan, J. Browse, K. J. Pringle, K. Ardon-Dryer, A. K. Bertram, S. M. Burrows, D. Ceburnis, P. J. Demott, R. H. Mason, C. D. O'Dowd, M. Rinaldi, K. S. Carslaw, Contribution of feldspar and marine organic aerosols to global ice nucleating particle concentrations. *Atmos. Chem. Phys.* **17**, 3637–3658 (2017).

32. S. Yadav, R. E. Venezia, R. W. Paerl, M. D. Petters, Characterization of ice-nucleating particles over Northern India. *J. Geophys. Res. Atmos*. **124**, 10467–10482 (2019).

33. G. C. Cornwell, C. M. Sultana, M. D. Petters, H. Al-Mashat, N. E. Rothfuss, O. Möhler, P. J. DeMott, A. C. Martin, K. A. Prather, Discrimination between individual dust and bioparticles using aerosol time-of-flight mass spectrometry. *Aerosol Sci. Tech.* **56**, 592–608 (2022).

34. T. P. Wright, J. D. Hader, G. R. McMeeking, M. D. Petters, High relative humidity as a trigger for widespread release of ice nuclei. *Aerosol. Sci. Tech.* **48**, i–v (2014).

35. K. J. Suski, T. C. J. Hill, E. J. T. Levin, A. Miller, P. J. DeMott, S. M. Kreidenweis, Agricultural harvesting emissions of ice-nucleating particles. *Atmos. Chem. Phys.* **18**, 13755–13771 (2018).

36. X. Gong, M. Radenz, H. Wex, P. Seifert, F. Ataei, S. Henning, H. Baars, B. Barja, A. Ansmann, F. Stratmann, Significant continental source of ice-nucleating particles at the tip of Chile's southernmost Patagonia region. *Atmos. Chem. Phys.* **22**, 10505–10525 (2022).

37. J. A. Huffman, A. J. Prenni, P. J. Demott, C. Pöhlker, R. H. Mason, N. H. Robinson, J. Fröhlich-Nowoisky, Y. Tobo, V. R. Després, E. Garcia, D. J. Gochis, E. Harris, I. Müller-Germann, C. Ruzene, B. Schmer, B. Sinha, D. A. Day, M. O. Andreae, J. L. Jimenez, M. Gallagher, S. M. Kreidenweis, A. K. Bertram, U. Pöschl, High concentrations of biological aerosol particles and ice nuclei during and after rain. *Atmos. Chem. Phys.* **13**, 6151–6164 (2013).

38. K. Hara, T. Maki, F. Kobayashi, M. Kakikawa, M. Wada, A. Matsuki, Variations of ice nuclei concentration induced by rain and snowfall within a local forested site in Japan. *Atmos. Environ.* **127**, 1–5 (2016).

39. C. M. Rathnayake, N. Metwali, T. Jayarathne, J. Kettler, Y. Huang, P. S. Thorne, P. T. O'Shaughnessy, E. A. Stone, Influence of rain on the abundance of bioaerosols in fine and coarse particles. *Atmos. Chem. Phys.* **17**, 2459–2475 (2017).

40. I. Pisso, E. Sollum, H. Grythe, N. I. Kristiansen, M. Cassiani, S. Eckhardt, D. Arnold, D. Morton, R. L. Thompson, C. D. Groot Zwaaftink, N. Evangeliou, H. Sodemann, L. Haimberger, S. Henne, D. Brunner, J. F. Burkhart, A. Fouilloux, J. Brioude, A. Philipp, P. Seibert, A. Stohl, The Lagrangian particle dispersion model FLEXPART version 10.4. *Geosci. Model Dev.* **12**, 4955–4997 (2019).

41. P. Seibert, A. Frank, Source-receptor matrix calculation with a Lagrangian particle dispersion model in backward mode. *Atmos. Chem. Phys.* **4**, 51–63 (2004).

42. S. M. Burrows, T. Butler, P. Jöckel, H. Tost, A. Kerkweg, U. Pöschl, M. G. Lawrence, Bacteria in the global atmosphere–Part 2: Modeling of emissions and transport between different ecosystems. *Atmos. Chem. Phys.* **9**, 9281–9297 (2009).

43. R. H. H. Janssen, C. L. Heald, A. L. Steiner, A. E. Perring, J. A. Huffman, E. S. Robinson, C. H. Twohy, L. D. Ziemba, Drivers of the fungal spore bioaerosol budget: Observational analysis and global modeling. *Atmos. Chem. Phys.* **21**, 4381–4401 (2021).

44. C. Hoose, O. Möhler, Heterogeneous ice nucleation on atmospheric aerosols: A review of results from laboratory experiments. *Atmos. Chem. Phys*. **12**, 9817–9854 (2012).

45. S. Patade, V. Phillips, S. M. Burrows, C. Morris, D. Knopf, P. Amato, F. Goncalves, H. Bingemer, J. Schrod, P. DeMott, C. Alwmark, C. Pöhlker, Empirical formulation for multiple groups of primary biological ice nuclei from field observations over Amazonia. *J. Atmos. Sci.* **78**, 2195–2220 (2021).

46. S. Augustin-Bauditz, H. Wex, S. Kanter, M. Ebert, D. Niedermeier, F. Stolz, A. Prager, F. Stratmann, The immersion mode ice nucleation behavior of mineral dusts: A comparison of different pure and surface modified dusts. *Geophys. Res. Lett.* **41**, 7375–7382 (2014).

47. L. G. Jahl, T. A. Brubaker, M. J. Polen, L. G. Jahn, K. P. Cain, B. B. Bowers, W. D. Fahy, S. Graves, R. C. Sullivan, Atmospheric aging enhances the ice nucleation ability of biomass-burning aerosol. *Sci. Adv.* **7**, eabd3440 (2021).

48. M. Joly, E. Attard, M. Sancelme, L. Deguillaume, C. Guilbaud, C. E. Morris, P. Amato, A.-M. Delort, Ice nucleation activity of bacteria isolated from cloud water. *Atmos. Environ.* **70**, 392–400 (2013).

49. B. G. Pummer, H. Bauer, J. Bernardi, S. Bleicher, H. Grothe, Suspendable macromolecules are responsible for ice nucleation activity of birch and conifer pollen. *Atmos. Chem. Phys.* **12**, 2541–2550 (2012).

50. K. Dietzel, D. Valle, N. Fierer, J. M. U'ren, A. Barberán, Geographical distribution of fungal plant pathogens in dust across the United States. *Front. Ecol. Evol.* **7**, 1–8 (2019).

51. A. Barberán, J. Ladau, J. W. Leff, K. S. Pollard, H. L. Menninger, R. R. Dunn, N. Fierer, Continental-scale distributions of dust-associated bacteria and fungi. *Proc. Natl. Acad. Sci. U.S.A.* **112**, 5756–5761 (2015).

52. E. Gute, R. O. David, Z. A. Kanji, J. P. D. Abbatt, Ice nucleation ability of tree pollen altered by atmospheric processing. *ACS Earth Space Chem.* **4**, 2312–2319 (2020).

53. P. T. Mckenney, A. Driks, P. Eichenberger, The *Bacillus subtilis* endospore: Assembly and functions of the multilayered coat. *Nat. Rev. Microbiol.* **11**, 33–44 (2013).

54. P. Roy, L. E. Mael, T. C. J. Hill, L. Mehndiratta, G. Peiker, M. L. House, P. J. DeMott, V. H. Grassian, C. S. Dutcher, Ice nucleating activity and residual particle morphology of bulk seawater and sea surface microlayer. *ACS Earth Space Chem.* **5**, 1916–1928 (2021).

55. C. H. Twohy, G. R. McMeeking, P. J. DeMott, C. S. McCluskey, T. C. J. Hill, S. M. Burrows, G. R. Kulkarni, M. Tanarhte, D. N. Kafle, D. W. Toohey, Abundance of fluorescent biological aerosol particles at temperatures conducive to the formation of mixed-phase and cirrus clouds. *Atmos. Chem. Phys.* **16**, 8205–8225 (2016).

56. A. E. Perring, J. P. Schwarz, D. Baumgardner, M. T. Hernandez, D. V. Spracklen, C. L. Heald, R. S. Gao, G. Kok, G. R. McMeeking, J. B. McQuaid, D. W. Fahey, Airborne observations of regional variation in fluorescent aerosol across the United States. *J. Geophys. Res. Atmos*. **120**, 1153–1170 (2015).

57. K. C. Failor, D. G. Schmale, B. A. Vinatzer, C. L. Monteil, Ice nucleation active bacteria in precipitation are genetically diverse and nucleate ice by employing different mechanisms. *ISME J.* **11**, 2740–2753 (2017).

58. S. Yadav, N. P. Curtis, R. E. Venezia, A. Tandon, R. W. Paerl, M. D. Petters, Bioaerosol diversity and ice nucleating particles in the North-Western Himalayan region. *J. Geophys. Res. Atmospheres*, **127**, e2021JD036299 (2022).

59. B. H. Matthews, A. N. Alsante, S. D. Brooks, Pollen emissions of subpollen particles and ice nucleating particles. *ACS Earth Space Chem.* **7**, 1207–1218 (2023).

60. D. O'Sullivan, B. J. Murray, J. F. Ross, T. F. Whale, H. C. Price, J. D. Atkinson, N. S. Umo, M. E. Webb, The relevance of nanoscale biological fragments for ice nucleation in clouds. *Sci. Rep.* **5**, 1–7 (2015).

61. N. Hiranuma, O. Möhler, K. Yamashita, T. Tajiri, A. Saito, A. Kiselev, N. Hoffmann, C. Hoose, E. Jantsch, T. Koop, M. Murakami, Ice nucleation by cellulose and its potential contribution to ice formation in clouds. *Nat. Geosci.* **8**, 273–277 (2015).

62. C. S. McCluskey, T. C. J. Hill, C. M. Sultana, O. Laskina, J. Trueblood, M. V. Santander, C. M. Beall, J. M. Michaud, S. M. Kreidenweis, K. A. Prather, V. Grassian, P. J. DeMott, A mesocosm double feature: Insights into the chemical makeup of marine ice nucleating particles. *J. Atmos. Sci.* **75**, 2405–2423 (2018).

63. F. Conen, A. Einbock, C. Mignani, C. Hüglin, Measurement report: Ice-nucleating particles active ≥ −15 °C in free tropospheric air over western Europe. *Atmos. Chem. Phys.* **22**, 3433–3444 (2022).

64. J. M. Creamean, K. Barry, T. C. J. Hill, C. Hume, P. J. DeMott, M. D. Shupe, S. Dahlke, S. Willmes, J. Schmale, I. Beck, C. J. M. Hoppe, A. Fong, E. Chamberlain, J. Bowman, R. Scharien, O. Persson, Annual cycle observations of aerosols capable of ice formation in central Arctic clouds. *Nat. Commun.* **13**, 3537 (2022).

65. A. C. Martin, G. C. Cornwell, S. A. Atwood, K. A. Moore, N. E. Rothfuss, H. Taylor, P. J. DeMott, S. M. Kreidenweis, M. D. Petters, K. A. Prather, Transport of pollution to a remote coastal site during gap flow from California's interior: Impacts on aerosol composition, clouds, and radiative balance. *Atmos. Chem. Phys.* **17**, 1491–1509 (2017).

66. G. Vali, Quantitative evaluation of experimental results an the heterogeneous freezing nucleation of supercooled liquids. *J. Atmos. Sci.* **28**, 402–409 (1971).

67. A. Agresti, B. A. Coull, Approximate is better than "exact" for interval estimation of binomial proportions. *Am. Stat.* **52**, 119–126 (1998).

68. A. M. Gabey, W. R. Stanley, M. W. Gallagher, P. H. Kaye, The fluorescence properties of aerosol larger than 0.8 μ in urban and tropical rainforest locations. *Atmos. Chem. Phys.* **11**, 5491–5504 (2011).

69. N. J. Savage, C. E. Krentz, T. Könemann, T. T. Han, G. Mainelis, C. Pöhlker, J. Alex Huffman, Systematic characterization and fluorescence threshold strategies for the wideband integrated bioaerosol sensor (WIBS) using size-resolved biological and interfering particles. *Meas. Tech.* **10**, 4279–4302 (2017).

70. C. M. Sultana, G. C. Cornwell, P. Rodriguez, K. A. Prather, FATES: A flexible analysis toolkit for the exploration of single-particle mass spectrometer data. *Atmos. Meas. Tech.* **10**, 1323–1334 (2017).

71. X. H. Song, P. K. Hopke, D. P. Fergenson, K. a. Prather, Classification of single particles analyzed by ATOFMS using an artificial neural network, ART-2A. *Anal. Chem.* **71**, 860–865 (1999).

72. P. A. Alpert, D. A. Knopf, Analysis of isothermal and cooling-rate-dependent immersion freezing by a unifying stochastic ice nucleation model. *Atmos. Chem. Phys*. **16**, 2083–2107 (2016).

73. D. A. Knopf, P. A. Alpert, A. Zipori, N. Reicher, Y. Rudich, Stochastic nucleation processes and substrate abundance explain time-dependent freezing in supercooled droplets. *Npj Clim. Atmos. Sci.* **3**, 1–9 (2020).

74. X. Qin, P. V. Bhave, K. A. Prather, Comparison of two methods for obtaining quantitative mass concentrations from aerosol time-of-flight mass spectrometry measurements. *Anal. Chem.* **78**, 6169–6178 (2006).

75. J. M. Alexander, D. M. Bell, D. Imre, P. D. Kleiber, V. H. Grassian, A. Zelenyuk, D. M. Bell, D. Imre, P. D. Kleiber, V. H. Grassian, Measurement of size-dependent dynamic shape factors of quartz particles in two flow regimes. *Aerosol. Sci. Tech.* **50**, 870–879 (2016).

76. D. J. Cziczo, P. J. DeMott, C. Brock, P. K. Hudson, B. Jesse, S. M. Kreidenweis, A. J. Prenni, J. Schreiner, D. S. Thomson, D. M. Murphy, A method for single particle mass spectrometry of ice nuclei. *Aerosol. Sci. Tech.* **37**, 460–470 (2003).

77. T. Eidhammer, P. J. DeMott, S. M. Kreidenweis, A comparison of heterogeneous ice nucleation parameterizations using a parcel model framework. *J. Geophys. Res.* **114**, D06202 (2009).

78. P. J. DeMott, A. J. Prenni, G. R. McMeeking, R. C. Sullivan, M. D. Petters, Y. Tobo, M. Niemand, O. Möhler, J. R. Snider, Z. Wang, S. M. Kreidenweis, Integrating laboratory and field data to quantify the immersion freezing ice nucleation activity of mineral dust particles. *Atmos. Chem. Phys.* **15**, 393–409 (2015).

79. J. C. Golaz, P. M. Caldwell, L. P. Van Roekel, M. R. Petersen, Q. Tang, J. D. Wolfe, G. Abeshu, V. Anantharaj, X. S. Asay-Davis, D. C. Bader, S. A. Baldwin, G. Bisht, P. A. Bogenschutz, M. Branstetter, M. A. Brunke, S. R. Brus, S. M. Burrows, P. J. Cameron-Smith, A. S. Donahue, M. Deakin, R. C. Easter, K. J. Evans, Y. Feng, M. Flanner, J. G. Foucar, J. G. Fyke, B. M. Griffin, C. Hannay, B. E. Harrop, M. J. Hoffman, E. C. Hunke, R. L. Jacob, D. W. Jacobsen, N. Jeffery, P. W. Jones, N. D. Keen, S. A. Klein, V. E. Larson, L. R. Leung, H. Y. Li, W. Lin, W. H. Lipscomb, P. L. Ma, S. Mahajan, M. E. Maltrud, A. Mametjanov, J. L. McClean, R. B. McCoy, R. B. Neale, S. F. Price, Y. Qian, P. J. Rasch, J. E. J. R. Eyre, W. J. Riley, T. D. Ringler, A. F. Roberts, E. L. Roesler, A. G. Salinger, Z. Shaheen, X. Shi, B. Singh, J. Tang, M. A. Taylor, P. E. Thornton, A. K. Turner, M. Veneziani, H. Wan, H. Wang, S. Wang, D. N. Williams, P. J. Wolfram, P. H. Worley, S. Xie, Y. Yang, J. H. Yoon, M. D. Zelinka, C. S. Zender, X. Zeng, C. Zhang, K. Zhang, Y. Zhang, X. Zheng, T. Zhou, Q. Zhu, The DOE E3SM coupled model version 1: Overview and evaluation at standard resolution. *J. Adv. Model. Earth Syst.* **11**, 2089–2129 (2019).

80. P. J. Rasch, S. Xie, P. L. Ma, W. Lin, H. Wang, Q. Tang, S. M. Burrows, P. Caldwell, K. Zhang, R. C. Easter, P. Cameron-Smith, B. Singh, H. Wan, J. C. Golaz, B. E. Harrop, E. Roesler, J. Bacmeister, V. E. Larson, K. J. Evans, Y. Qian, M. Taylor, L. R. Leung, Y. Zhang, L. Brent, M. Branstetter, C. Hannay, S. Mahajan, A. Mametjanov, R. Neale, J. H. Richter, J. H. Yoon, C. S. Zender, D. Bader, M. Flanner, J. G. Foucar, R. Jacob, N. Keen, S. A. Klein, X. Liu, A. G. Salinger, M. Shrivastava, Y. Yang, An overview of the atmospheric component of the energy exascale earth system model. *J. Adv. Model. Earth Syst.* **11**, 2377–2411 (2019).

81. P. J. Lawrence, T. N. Chase, Representing a new MODIS consistent land surface in the Community Land Model (CLM 3.0). *J. Geophys. Res.* **112**, G01023 (2007).

82. R. Gelaro, W. McCarty, M. J. Suárez, R. Todling, A. Molod, L. Takacs, C. A. Randles, A. Darmenov, M. G. Bosilovich, R. Reichle, K. Wargan, L. Coy, R. Cullather, C. Draper, S. Akella, V. Buchard, A. Conaty, A. M. da Silva, W. Gu, G. K. Kim, R. Koster, R. Lucchesi, D. Merkova, J. E. Nielsen, G. Partyka, S. Pawson, W. Putman, M. Rienecker, S. D. Schubert, M. Sienkiewicz, B. Zhao, The modern-era retrospective analysis for research and applications, version 2 (MERRA-2). *J. Climate* **30**, 5419–5454 (2017).

83. P. L. Ma, P. J. Rasch, M. Wang, H. Wang, S. J. Ghan, R. C. Easter, W. I. Gustafson, X. Liu, Y. Zhang, H. Y. Ma, How does increasing horizontal resolution in a global climate model improve the simulation of aerosol-cloud interactions? *Geophys. Res. Lett.* **42**, 5058–5065 (2015).

84. J. Sun, K. Zhang, H. Wan, P. Ma, Q. Tang, S. Zhang, Impact of nudging strategy on the climate representativeness and hindcast skill of constrained EAMv1 simulations. *J. Adv. Model. Earth Syst.* **11**, 3911–3933 (2019).

85. X. Liu, P. L. Ma, H. Wang, S. Tilmes, B. Singh, R. C. Easter, S. J. Ghan, P. J. Rasch, Description and evaluation of a new four-mode version of the Modal Aerosol Module (MAM4) within version 5.3 of the community atmosphere model. *Geosci. Model Dev.* **9**, 505–522 (2016).

86. H. Wang, R. C. Easter, R. Zhang, P. Ma, B. Singh, K. Zhang, D. Ganguly, P. J. Rasch, S. M. Burrows, S. J. Ghan, S. Lou, Y. Qian, Y. Yang, Y. Feng, M. Flanner, L. R. Leung, X. Liu, M. Shrivastava, J. Sun, Q. Tang, S. Xie, J. Yoon, Aerosols in the E3SM version 1: New developments and their impacts on radiative forcing. *J. Adv. Model. Earth Syst.* **12**, e2019MS001851 (2020).

87. C. S. Zender, H. Bian, B. Newman, Mineral Dust Entrainment and Deposition (DEAD) model: Description and 1990s dust climatology. *J. Geophys. Res. Atmospheres* **108**, 4416 (2003).

88. E. M. Mårtensson, E. D. Nilsson, G. de Leeuw, L. H. Cohen, H. C. Hansson, Laboratory simulations and parameterization of the primary marine aerosol production. *J. Geophys. Res. Atmos*. **108**, 1–12 (2003).

89. E. C. Monahan, D. E. Spiel, K. L. Davidson, A model of marine aerosol generation via whitecaps and wave disruption, in *Oceanic Whitecaps*, E. C. Monahan, G. M. Niocaill, Eds. (Springer Netherlands, 1986), vol. 2 of Oceanographic Sciences Library, pp. 167–174.

90. S. M. Burrows, O. Ogunro, A. A. Frossard, L. M. Russell, P. J. Rasch, S. M. Elliott, A physically based framework for modeling the organic fractionation of sea spray aerosol from bubble film Langmuir equilibria. *Atmos. Chem. Phys.* **14**, 13601–13629 (2014).

91. J. Brioude, D. Arnold, A. Stohl, M. Cassiani, D. Morton, P. Seibert, W. Angevine, S. Evan, A. Dingwell, J. D. Fast, R. C. Easter, I. Pisso, J. Burkhart, G. Wotawa, The Lagrangian particle dispersion model FLEXPART-WRF version 3.1. *Geosci. Model Dev.* **6**, 1889–1904 (2013).

92. W. C. Skamarock, J. B. Klemp, J. Dudhi, D. O. Gill, D. M. Barker, M. G. Duda, X.-Y. Huang, W. Wang, J. G. Powers, "A description of the advanced research WRF version 3" (NCAR Technical Note, 2008), p. 113.

93. G. Thompson, P. R. Field, R. M. Rasmussen, W. D. Hall, Explicit forecasts of winter precipitation using an improved bulk microphysics scheme. Part II: Implementation of a new snow parameterization. *Mon. Weather Rev.* **136**, 5095–5115 (2008).

94. M. Nakanishi, H. Niino, Development of an improved turbulence closure model for the atmospheric boundary layer. *J. Meteorol. Soc. Jpn. Ser.* **87**, 895–912 (2009).

95. Z. Janjić, "Nonsingular implementation of the Mellor-Yamada level 2.5 scheme in the NCEP Meso model" (Office Note, National Centers for Environmental Prediction, 2001).

96. F. Chen, J. Dudhia, Coupling an advanced land surface–hydrology model with the Penn State–NCAR MM5 modeling system. Part I: Model implementation and sensitivity. *Mon. Weather Rev.* **129**, 569–585 (2001).

97. M. J. Iacono, J. S. Delamere, E. J. Mlawer, M. W. Shephard, S. A. Clough, W. D. Collins, Radiative forcing by long-lived greenhouse gases: Calculations with the AER radiative transfer models. *J. Geophys. Res. Atmos*. **113**, 2–9 (2008).

98. H. Shao, J. Derber, X.-Y. Huang, M. Hu, K. Newman, D. Stark, M. Lueken, C. Zhou, L. Nance, Y.-H. Kuo, B. Brown, Bridging research to operations transitions: Status and plans of community GSI. *Bull. Am. Meteorol. Soc.* **97**, 1427–1440 (2016).

99. S. L. Tai, Z. Feng, P. L. Ma, C. Schumacher, J. D. Fast, Representations of precipitation diurnal cycle in the amazon as simulated by observationally constrained cloud-system resolving and global climate models. *J. Adv. Model. Earth Syst.* **13**, 1–25 (2021).

100. R. Myneni, Y. Knyazikhin, T. Park, MCD15A3H MODIS/Terra+Aqua Leaf Area Index/FPAR 4-day L4 Global 500m SIN Grid V006 [Data set]. NASA EOSDIS Land Processes DAAC. (2015); doi:10.5067/MO1DIS/MCD15A3H.006.

101. D. W. Griffin, C. Gonzalez, N. Teigell, T. Petrosky, D. E. Northup, M. Lyles, Observations on the use of membrane filtration and liquid impingement to collect airborne microorganisms in various atmospheric environments. *Aerobiologia* **27**, 25–35 (2011).

102. Z. Wang, T. Reponen, S. A. Grinshpun, R. L. Górny, K. Willeke, Effect of sampling time and air humidity on the bioefficiency of filter samplers for bioaerosol collection. *J. Aerosol Sci.* **32**, 661–674 (2001).

103. P. J. DeMott, T. C. J. Hill, M. D. Petters, A. K. Bertram, Y. Tobo, R. H. Mason, K. J. Suski, C. S. McCluskey, E. J. T. Levin, G. P. Schill, Y. Boose, A. M. Rauker, A. J. Miller, J. Zaragoza, K. Rocci, N. E. Rothfuss, H. P. Taylor, J. D. Hader, C. Chou, J. A. Huffman, U. Pöschl, A. J. Prenni, S. M. Kreidenweis, Comparative measurements of ambient atmospheric concentrations of ice nucleating particles using multiple immersion freezing methods and a continuous flow diffusion chamber. *Atmos. Chem. Phys.* **17**, 11227–11245 (2017).

104. P. J. DeMott, O. Möhler, D. J. Cziczo, N. Hiranuma, M. D. Petters, S. S. Petters, F. Belosi, H. G. Bingemer, S. D. Brooks, C. Budke, M. Burkert-Kohn, K. N. Collier, A. Danielczok, O. Eppers, L. Felgitsch, S. Garimella, H. Grothe, P. Herenz, T. C. J. Hill, K. Höhler, Z. A. Kanji, A. Kiselev, T. Koop, T. B. Kristensen, K. Krüger, G. Kulkarni, E. J. T. Levin, B. J. Murray, A. Nicosia, D. O'Sullivan, A. Peckhaus, M. J. Polen, H. C. Price, N. Reicher, D. A. Rothenberg, Y. Rudich, G. Santachiara, T. Schiebel, J. Schrod, T. M. Seifried, F. Stratmann, R. C. Sullivan, K. J. Suski, M. Szakáll, H. P. Taylor, R. Ullrich, J. Vergara-Temprado, R. Wagner, T. F. Whale, D. Weber, A. Welti, T. W. Wilson, M. J. Wolf, J. Zenker, The Fifth International Workshop on Ice Nucleation phase 2 (FIN-02): Laboratory intercomparison of ice nucleation measurements. *Atmos. Meas. Tech.* **11**, 6231–6257 (2018).

105. N. Hiranuma, S. Augustin-Bauditz, H. Bingemer, C. Budke, J. Curtius, A. Danielczok, K. Diehl, K. Dreischmeier, M. Ebert, F. Frank, N. Hoffmann, K. Kandler, A. Kiselev, T. Koop, T. Leisner, O. Möhler, B. Nillius, A. Peckhaus, D. Rose, S. Weinbruch, H. Wex, Y. Boose, P. J. Demott, J. D. Hader, T. C. J. Hill, Z. A. Kanji, G. Kulkarni, E. J. T. Levin, C. S. McCluskey, M. Murakami, B. J. Murray, D. Niedermeier, M. D. Petters, D. O'Sullivan, A. Saito, G. P. Schill, T. Tajiri, M. A. Tolbert, A. Welti, T. F. Whale, T. P. Wright, K. Yamashita, A comprehensive laboratory study on the immersion freezing behavior of illite NX particles: A comparison of 17 ice nucleation measurement techniques. *Atmos. Chem. Phys.* **15**, 2489–2518 (2015).

106. V. Huijnen, H. Eskes, Skill scores and evaluation methodology for the MACC II project. *MACC-II Deliv. D85* **2** (2012).